HHS Public Access

Author manuscript

Int J Min Sci Technol. Author manuscript; available in PMC 2018 February 05.

Published in final edited form as:

Int J Min Sci Technol. 2018 January ; 28(1): 137–144. doi:10.1016/j.ijmst.2017.10.003.

Applying robust design to study the effects of stratigraphic characteristics on brittle failure and bump potential in a coal mine

Bo-Hyun Kim[*], **Mark K. Larson**, and **Heather E. Lawson**

Spokane Mining Research Division, NIOSH/CDC, Spokane, WA 99207, USA

Abstract

Bumps and other types of dynamic failure have been a persistent, worldwide problem in the underground coal mining industry, spanning decades. For example, in just five states in the U.S. from 1983 to 2014, there were 388 reportable bumps. Despite significant advances in mine design tools and mining practices, these events continue to occur. Many conditions have been associated with bump potential, such as the presence of stiff units in the local geology. The effect of a stiff sandstone unit on the potential for coal bumps depends on the location of the stiff unit in the stratigraphic column, the relative stiffness and strength of other structural members, and stress concentrations caused by mining. This study describes the results of a robust design to consider the impact of different lithologic risk factors impacting dynamic failure risk. Because the inherent variability of stratigraphic characteristics in sedimentary formations, such as thickness, engineering material properties, and location, is significant and the number of influential parameters in determining a parametric study is large, it is impractical to consider every simulation case by varying each parameter individually. Therefore, to save time and honor the statistical distributions of the parameters, it is necessary to develop a robust design to collect sufficient sample data and develop a statistical analysis method to draw accurate conclusions from the collected data. In this study, orthogonal arrays, which were developed using the robust design, are used to define the combination of the (a) thickness of a stiff sandstone inserted on the top and bottom of a coal seam in a massive shale mine roof and floor, (b) location of the stiff sandstone inserted on the top and bottom of the coal seam, and (c) material properties of the stiff sandstone and contacts as interfaces using the 3-dimensional numerical model, FLAC3D. After completion of the numerical experiments, statistical and multivariate analysis are performed using the calculated results from the orthogonal arrays to analyze the effect of these variables. As a consequence, the impact of each of the parameters on the potential for bumps is quantitatively classified in terms of a normalized intensity of plastic dissipated energy. By multiple regression, the intensity of plastic dissipated energy and migration of the risk from the roof to the floor via the pillars is predicted based on the value of the variables. The results demonstrate and suggest a possible capability to predict the bump potential in a given rock mass adjacent to the underground

[*]Corresponding author: ljn0@cdc.gov (B.-H. Kim).

Disclaimer

The findings and conclusions in this report are those of the authors and do not necessarily represent the views of the National Institute for Occupational Safety and Health. Mention of any company or product does not constitute endorsement by NIOSH.

excavations and pillars. Assessing the risk of bumps is important to preventing fatalities and injuries resulting from bumps.

Keywords

Bumps; Robust design; FLAC3D; Plastic dissipated energy; Multiple regression

1. Introduction

This paper is developed as part of an effort by the National Institute for Occupational Safety and Health (NIOSH) to identify risk factors associated with bumps in order to prevent fatalities and accidents in highly stressed, bump-prone ground conditions. The main objective of this study is to demonstrate the application of a robust design procedure by using factors affecting coal bumps based on the previous works by Lawson et al. as an example application [1,2]. The type of catastrophic failure in coal mines known as dynamic failure—also colloquially referred to as bumps, bounces, bursts, and others—is one of the most challenging and persistent safety and engineering problems associated with coal mining in highly stressed conditions. Coal pillar bursts involve the sudden expulsion of coal and rock into the mine opening. These events occur when stresses in a coal pillar, left for support in underground workings, exceed the critical strength capacity of the pillar, causing it to rupture without warning. Agapito and Goodrich investigate five common stress factors responsible for bump problems in Utah—depth of cover, sandstone channels, arching of strata, faults, and coal seam thickness—and find that these factors can concentrate or relieve stress to affect the potential for bumps [3]. In addition, floor failure in a coal mine often inhibits longwall mining when large displacement of floor strata, known as floor heave, interferes with travel, access, ventilation, and equipment. Aggson investigates floor heave in West Virginia where an underclay is relatively strong and high horizontal stress persists, and reported that the failure mode manifests mainly by buckling rather than by plastic flow [4]. Lawson et al. conduct a study of the effect of a stiff sandstone member in the near-seam overburden on the potential for shock bumps [1,2]. They find that the effect of the stiff sandstone unit on large-scale roof failure and potential for coal bumps depends on the location of the stiff unit in the stratigraphic column, the relative stiffness and strength of other structural members, and stress concentrations caused by mining. A correlation between bumping behavior and the ratio of stiff-to-compliant strata is observed empirically through examination of core logs, and it is shown that the relative influence of a stiff beam member is heavily impacted by the nature of the surrounding strata. However, a concise and broadly applicable relationship of coal bump potential to the ratio of the overall stiff-to-compliant strata alone is not clearly demonstrated by the investigation. Instead, the study suggests that site-specific modeling be conducted, using detailed local geology—a time-consuming approach that requires extensive modeling capability and geologic reconnaissance, which may or may not be practical for a given mine. Many uncertainties remain in the highly stressed coal seams associated with geologic structure and spatial redistribution of induced stress in coal pillars and adjacent to the mine openings due to coal extraction. Thus, to prevent fatalities in underground coal mining, a continuous effort is required to better understand the catastrophic failure mechanism in coal mines.

A robust design (the Taguchi method [5,6] along with FLAC3D [7]) is used in this study to predict bump potential associated with plastic dissipated energy in a highly stressed coal pillar with respect to the stratigraphic characteristics of sedimentary formation, such as thickness, engineering material properties, and location. Because the inherent variability of the significant factors is substantial and the number of influential parameters in determining a parametric study is large, it is impractical to consider every simulation case by varying each parameter individually. Statistical experimental design is widely used to assist in data acquisition, decrease experiment error, and provide statistical analysis tools to describe the degree of errors. In statistical experimental design, two basic principles—replication and randomness—are required. Replication means that the same results can be obtained by the same experimental conditions. Randomness is required to ensure objectivity by putting the experimental objects into different conditions or by randomly arranging their experimental order. Furthermore, it is necessary to have a homogeneous experimental environment when applying the probability theory [8,9]. The Taguchi method was developed based on orthogonal array experiments. This gives a much reduced variance for the experiment with optimum settings of control parameters.

Orthogonal arrays provide a set of well-balanced (or minimum) experiments and serve as objective functions for optimization. The aim is to reduce the number of experiments in order to minimize the resources such as equipment, materials, manpower, or time. However, doing all of the factorial experiments is suitable when conducting experiments is cheap and quick but measurements are expensive and take too long, and when the experimental facility will not be available later to conduct the verification experiment. Conducting separate experiments for studying interactions between factors is not desirable. The general steps involved in the Taguchi method are as follows: (1) define the process objective, or more specifically, a target value for a performance measure of the process, and (2) determine the design parameters affecting the process. The number of levels that the parameters should be varied at must be specified in order to: (1) create orthogonal arrays for the parameter design indicating the number of and conditions for each experiment. The selection of orthogonal arrays is based on the number of parameters and the levels of variation for each parameter, and will be expounded; (2) conduct the experiments indicated in the completed array to collect data on the effect on the performance measure; and finally (3) complete data analysis to determine the effect of the different parameters on the performance measure.

The effect of many different factors on the performance characteristic in a condensed set of experiments can be examined by using the orthogonal array experimental design. The levels at which these parameters should be varied must be determined. Determining what levels of a variable to test requires an indepth understanding of the process, including the minimum, maximum, and current value of the parameter. Orthogonal arrays created by the robust design are used to define the combination of the (a) thickness of a stiff sandstone inserted on the top and bottom of a coal seam in a massive shale mine roof and floor, (b) location of the stiff sandstone inserted on the top and bottom of the coal seam, and (c) material properties of the stiff sandstone and contacts as interfaces using FLAC3D. When there are many parameters to be studied, the main effect of each parameter and some of the reciprocal actions are estimated, while other reciprocal actions are disregarded to reduce the number of tests. The benefits of orthogonal array design are that it calculates the parameter changes

from experimental or field-mapping data, facilitates the easy preparation of input data for analysis of variance, and accommodates many parameters in experiments or simulations without increasing the test scale [8,9]. Assuming that there is an orthogonal array presented as $L_{25}(5^6)$, this means that six parameters can be used in the experiment, and there are five stages in which the parameter values can be varied. In this case, 15,625(=5^6) experiments in total are required to obtain results that are statistically significant and representative. If the orthogonal array is used, however, only 25 experiments are needed. After completion of the numerical experiments, multivariate analysis, such as principal component analysis and multiple regression, is performed using the calculated results from the orthogonal arrays. The effect of each variable on the intensity of dissipated plastic energy and consequent retained potential energy are investigated and quantified in order to predict the bump potential in the roof, floor, and pillars. In short, this method provides an efficient, practical way to estimate the amount of energy retained in the rock mass that may be subsequently released in the form of a dynamic failure event.

The next section introduces stochastic simulation for the estimation of engineering properties of the rock masses and describes the FLAC3D modeling approach, including assumptions and conditions. Finally, methodologies appropriate to evaluate the bump potential adjacent to the underground excavations and in the coal pillar are explained and demonstrated by means of the robust design and numerical modeling technique.

2. Assumptions and conditions for FLAC3D modeling for evaluation of the bump potential

2.1. Stochastic simulation for estimation of engineering properties of coal

For this study, the engineering material properties for the sandstone, the coal seam, and other lithologies which are modeled as an elasto-plastic model are estimated using the geological strength index (GSI). A stochastic approach is used to estimate the rock mass strength for the FLAC3D modeling. Monte Carlo simulations are used to obtain statistical distributions of engineering material properties of rock mass strength, based on the Hoek-Brown strength criterion using the available geotechnical data. The GSI, illustrated in Fig. 1, is proposed for heterogeneous rock masses by Marinos and Hoek, and provides an effective and meaningful way to estimate the strength of different rock types in lieu of laboratory testing [10].

Harr provides some coefficients of variation for parameters common to civil engineering design [11]. The coefficient of variation (CV) expresses a measure of the reliability of the central tendency. It is defined as the ratio of standard deviation to mean. For example, given a mean value of a parameter of 10 with a coefficient of variation of 10%, the CV would specify a standard deviation of 1. The higher the coefficient of variation, the greater will be the scatter. In this study, a CV of 40% for strength (cohesion) was used as a guide recommended by Harr in assigning the variability (i.e., standard deviation) of intact unconfined compressive strength (UCS) [11]. The typical range of moduli and strengths of both sandstone and coal proposed by Farmer, along with the 40% of CV, were considered [12]. For instance, the normal distribution of intact UCS for coal (28 ± 11 MPa) and intact Young's modulus for sandstone (38 ± 15 GPa) are provided to the Monte Carlo simulation.

Fig. 2 presents the examples of cumulative distribution of parameters as input data for the Monte Carlo simulation. The normal distribution of intact UCS for coal can be generated as shown in Fig. 2a. The triangular distribution of GSI for the rock mass (min: 20; most often: 27; max: 35), based on the description by the GSI chart, was considered as illustrated in Fig. 2b.

The Monte Carlo simulations are accomplished with the @Risk® software, using the methodology proposed by Hoek et al., to determine a value of the engineering material properties (i.e., modulus and strength parameters associated with variability) [13,14]. The methodology will not be discussed in detail here because it is beyond the scope of this paper. Fig. 3 presents the examples of results estimated by the Monte Carlo simulations. The cumulative distributions of cohesion and internal friction angle for the rock mass are illustrated in Fig. 3a and b, respectively. The cumulative distribution of the internal friction angle has plateaus since the input for the Hoek-Brown constant (m_i) is considered as a discrete distribution representing relatively less and more brittle and normal behavior.

Quantitative values of the engineering material properties in terms of percentiles from 5% to 95% for the rock masses were estimated by the Monte Carlo simulations using the software @Risk. The representative values of each engineering material property for sandstone and coal seam and rock masses are summarized in Table 1. As the input data for the numerical study, the 30th percentile of each engineering material property estimated by the simulation was chosen as a relatively conservative value from the point of view of safety. The results for the cohesion and internal friction angle are rounded to the nearest whole number.

2.2. Assumptions and input data for FLAC3D modeling on numerical experiments

A FLAC3D model with dimensions of 476 m (W) × 368 m (H) × 10 m (L) was constructed, simulating a longwall mine gateroad similar to that considered for the study of brittle failure mechanism by Kim and Larson [15]. A thickness of 182 m was used for the uppermost rock layer. The coal seam was 4 m thick. The lowermost layer was 178 m thick. The generalized ubiquitous-joint model (SUBI) was chosen as a constitutive model for this simulation [7]. The in-situ stress conditions used in this study were the same as those assumed for the characterization of bump-prone potential. The depth of the top boundary of the model from the surface was assumed to be 474.4 m below the surface. A surcharge of vertical stress was applied on the top boundary of the model to account for the weight of overburden not represented in the model. The horizontal stresses were considered to be greater than the vertical stress. It was presumed that the major principal stress (σ_H) had a magnitude (MPa) of 3.5× overburden in the *y*-direction of the model. The intermediate principal stress (σ_h) had a magnitude (MPa) of 2.5× overburden in the *x*-direction of the model. The minor principal stress (σ_v) had a magnitude (MPa) of the unit weight × depth [16].

For the boundary condition, both sides of the model were fixed in the *x*-direction, and both the front and back of the model were fixed in the *y*-direction. The bottom of the model was fixed in the *z*-direction. The geometries of the gate roads and pillars were simplified so that the gate road entries were 6 m wide and 4 m high, leaving pillars that were 22 and 52 m wide. Based on this robust design, an orthogonal array, $L_{25}(5^6)$, was prepared to consider the (a) thickness of a stiff sandstone inserted on the top and bottom of a coal seam in a massive

shale mine roof and floor, (b) location of the stiff sandstone inserted on the top and bottom of the coal seam, and (c) the elastic modulus of the sandstone and friction angle of the interfaces with five levels, respectively. This resulted in an orthogonal array that contained 25 numerical experiments, as shown in Table 2. Fig. 4 shows the examples of the FLAC3D model as the experimental cases 1 (sandstones adjacent to the seam) and 16 selected among the 25 cases by the orthogonal array.

2.3. Energy calculation in FLAC3D

Kim and Larson investigated and reported that the floor-heave and no floor-heave phenomenon associated with brittle failure in bump-prone ground was demonstrated by comparing the depth of floor yield in the vicinity of the gate roads, vertical displacement measured of the floor, and the ratio of elastic-to-dissipated plastic energy [15]. The floor heave causes significant loss of confinement in the pillar and increases the risk of a bump.

In this study, it is assumed that, if the magnitude of plastic dissipated energy working to fail the rock mass in the vicinity of underground excavation is greater than that of the baseline case (Case 1 in which all the properties are considered to be the default values), the risk of a bump in the rock mass would be relatively increased. In FLAC3D, elastic strain energy and dissipated plastic energy can be tracked for zones containing a mechanical model. FLAC3D uses an incremental solution procedure—i.e., the equations of motion at the grid points and the stress-strain calculations at the zones are solved at every time step. In the stress-strain equations, the incremental change in energy components is determined and accumulated as the system attempts to reach equilibrium. Energy is dissipated through plastic work as the zones undergo irreversible deformation based on the input material properties. Using FLAC3D, the strain in any zone can be divided into elastic and plastic parts [7].

3. Results and discussion

The geometries of the gate roads and pillars used in this study are simplified so that the gate road entries are 6 m wide and 4 m high, leaving pillars that are 22 m (narrow pillar) and 52 m wide (wide pillar). In the discussion of Figs. 5–10, the term “narrow” roof and floor refers to the roof and floor associated with the narrow, 22-m-wide pillars. The term “wide” roof and floor refers to the wide, 52-m-wide pillars.

Figs. 5–10 show the contours of dissipated plastic energy calculated by the FLAC3D for cases 7, 15, 21, 9, 8, and 5, respectively. The hotter color (orange-red) in the contours indicates a greater magnitude of dissipated plastic energy representing a higher risk of bumps. The dark-black bands in Figs. 5–10 represent the location and thickness of the stiff sandstone units in the top and bottom rock masses. The location of the highest plastic dissipated energy indicated by the hotter color in the contours is different depending on the elastic modulus and the thickness and offset of the stiff sandstone units by the orthogonal array.

Fig. 5 shows the results of case 7, which resulted in the maximum plastic energy dissipated in the region of wide roof. The plastic energy released is 28% more than that released in the baseline, case 1. Fig. 6 illustrates the result of case 15, showing the maximum plastic energy

dissipated in the wide pillars. The plastic energy dissipated is18% more than the energy dissipated incase 1. Fig. 7 presents the results of case 21, showing the maximum plastic energy dissipated in the floors of gate roads with the wide pillars. In this case, 12% more plastic energy is released compared to case 1.

Compared to the results of case 1, the results for cases 9, 8, and 5 show that 7%, 8%, and 21% more plastic energy was released in the region of the gate roads with narrow pillars as shown in Fig. 8 (roof), Fig. 9 (pillar), and Fig. 10 (floor), respectively.

In order to evaluate the potential for bumps associated with plastic dissipated energy at the different locations, all of the results of the energy calculations from each case are normalized as a ratio to the results of case 1. Table 3 shows the results of the normalization. Based on the normalized factors, a coefficient of variation (CV) of each location for dissipated energy was calculated and is shown in Table 4. The largest CV appears as 0.457 for the energy dissipated in the roof of the gate roads with narrow pillars. The smallest CV is calculated as 0.145 for the energy dissipated in the pillars of gate roads with narrow pillars. This means that there is a relatively high risk of bumps in the narrow pillars independent of the spatial characteristics (thickness or location) of the stiff sandstone and other engineering parameters. However, bump potential in the roof of gate roads with narrow pillars is relatively sensitive to the variability of the parameters, and the risk would be subject to the thickness or location of the stiff sandstone or other parameters.

Lawson et al. report that both the thickness of a discrete stiff member and its distance to the seam must be considered to anticipate areas of elevated rupture-induced hazards [1,2]. However, they find that the application of the results are limited if the assumptions and conditions are outside of the case studies used in their investigation. The constraints of the application of their results are mainly due to univariate analysis. In this study, multivariate analyses (i.e., principal component analysis and multiple regression) are conducted in order to not only overcome that limitation, but also to universally predict the risk and how several parameters affect that risk.

Table 5 shows the result of the correlation by principal component analysis. There is a relatively strong correlation (indicated with bold, italic numbers) of the energy release between the wide pillars and the roofs, whereas the plastic energy dissipated in the narrow pillars correlates more with the floors. In other words, a change of bump potential associated with plastic dissipated energy can be influenced not only by the stratigraphic characteristics but also by the geometry of the pillars.

To learn more about the relationship between the given parameters and the bump potential, multiple regression is performed to predict the relative change of the risk based on the orthogonal array. By using Eqs. (1)–(6), a change of the risk at the different locations can be predicted as a ratio of intensity of plastic dissipated energy. All of the input parameters and the resulting plastic dissipated energy in the equations are normalized so that the relative amount of change can be estimated in the assumed and given conditions of bump-prone ground.

The individual ratio of plastic dissipated energy in terms of the intensity of energy release on the different locations can be characterized and quantified by the multiple regression. From the analysis, the shear strength of the adjacent contacts in terms of internal friction angle is, in general, the most critical parameter contributing to dissipation of the plastic energy no matter where it is adjacent to the gate roads. Also, the Young's modulus of the stiff sandstone significantly contributes to the energy release in the narrow pillar and floor and in the wide roof and floor. In addition, the intensity of plastic dissipated energy in the wide and narrow roof is substantially controlled by the distance of the top stiff sandstone. As a consequence, the risk of bumps associated with plastic dissipated energy in the pillars is primarily influenced by the strength characteristics of the adjacent contacts. The risk in the roof is mainly dictated by the stiffness of discrete stiff member and its distance from the coal seam. Both the strength characteristics of the adjacent contacts and the stiffness of discrete stiff member principally contribute to the risk in the floor, as shown by the following equations:

$$W_p\,(Wide\ Pillar)=0.006t_{sst}+0.002t_{ssb}+0.653\varnothing_{if}+0.004E_{ss}-0.002d_{sst}+0.002d_{ssb}\times(r^2=0.96) \quad (1)$$

$$W_p\,(Narrow\ Pillar)=-0.009t_{sst}+0.652\varnothing_{if}+0.047E_{ss}+0.002d_{sst}+0.001d_{ssb}\times(r^2=0.97) \quad (2)$$

$$W_p\,(Wide\ Roof)=-0.008t_{sst}-0.004t_{ssb}+0.548\varnothing_{if}+0.139E_{ss}-0.016d_{sst}-0.01d_{ssb}\times(r^2=0.90) \quad (3)$$

$$W_p\,(Narrow\ Roof)=-0.006t_{sst}+0.001t_{ssb}+0.509\varnothing_{if}+0.08E_{ss}-0.016d_{sst}-0.008d_{ssb}\times(r^2=0.85) \quad (4)$$

$$W_p\,(Wide\ Floor)=0.001t_{sst}+0.001t_{ssb}+0.519\varnothing_{if}+0.089E_{ss}+0.002d_{sst}+0.004d_{ssb}\times(r^2=0.93) \quad (5)$$

$$W_p\,(Narrow\ Floor) = 0.001t_{sst} + 0.005t_{ssb} + 0.498\varnothing_{if} + 0.087E_{ss} + 0.002d_{sst} + 0.01d_{ssb} \times (r^2 = 0.89) \quad (6)$$

where W_p is the plastic dissipated energy; t_{sst} the thickness of top stiff sandstone; t_{ssb} the thickness of bottom stiff sandstone; $\varnothing_{if}$ the internal friction angle of interface; E_{ss} the elastic modulus of stiff sandstone; d_{sst} the distance of stiff sandstone from roof; and d_{ssb} = distance of stiff sandstone from floor.

4. Concluding remarks

In this study, the effect of a stiff sandstone unit on the potential for dynamic failure is shown to depend on the location of the stiff unit in the stratigraphic column and the relative stiffness and strength of other structural members. These effects are investigated using a combination of statistical and numerical techniques. The results suggest that the robust experimental design is a practical and effective method with which to consider the impact of different lithologic risk factors impacting dynamic failure potential.

In summary, the following are the results of the numerical investigation using an orthogonal array and the FLAC3D software, and based on the assumptions and methodologies described herein:

1. A robust design (i.e., the Taguchi method) is a very useful tool to consider a large number of possible statistical scenarios for a given mine site. As the inherent variability of the independent parameters is significant and the number of influential parameters in determining a parametric study is large, this represents a significant advantage over individually varying each parameter.
2. The results of the FLAC3D model show that a change in plastic dissipated energy is significantly impacted by the stratigraphic and engineering characteristics of the rock mass.
3. According to this research, the risk of bumps in narrow pillars is relatively high and is independent of the thickness or location of stiff sandstone and other engineering parameters.
4. Compared to the baseline case conditions, the bump potential in the roof of gate roads with narrow pillars is more sensitive to the variability of the parameters. The risk is dependent on the thickness, location of the stiff sandstone, and other parameters.
5. Using the regression formulas, a change in the risk at the different locations can be predicted as a ratio of intensity of plastic dissipated energy.
6. The magnitude of plastic dissipated energy in the vicinity of mine openings appears to be a reasonable indicator of the higher potential for dynamic failure.

7. For future work, continuous investigations should be conducted to systematically quantify the risk of bump associated not only with the factor of safety in deep coal mines but also with a surveillance system for mining-induced seismicity.

This study illustrates a method with which to estimate risk for dynamic failure events as a function of changing conditions. The results of this study indicate that friction angle of the sliding surfaces greatly affects elevated risk. Periodic testing of those surfaces and observations of physical indicators of friction angle might be used to map areas or regions with elevated risk for bumps. The method can be applied to other geometries and conditions, such as different stratigraphy and ranges of material properties. A better understanding of risk is a very critical step in improving miner safety with respect to bump potential in coal mines.

References

1. Lawson, HE., Tesarik, D., Larson, MK., Abraham, H. Effects of overburden characteristics on dynamic failure in underground coal mining. Proceedings: 35th international conference on ground control in mining; Morgantown, WV. July 26–28; p. 26-39.
2. Lawson HE, Tesarik D, Larson MK, Abraham H. Effects of overburden characteristics on dynamic failure in underground coal mining. IJMST. 2017; 27:21–9.
3. Agapito, JFT., Goodrich, RR. Five stress factors conducive to bumps in Utah, USA, coal mines. Proceedings: 19th international conference on ground control in mining; Morgantown, WV. August 8–10; p. 93-100.
4. USBM. Report of Investigations 8274. Pittsburgh, PA: U.S. Department of the Interior, Bureau of Mines (USBM); 1978. Coal mine floor heave in the Beckley coalbed, an analysis; p. 35
5. Taguchi, G. Introduction to quality engineering: designing quality into products and processes. Tokyo: Asian Productivity Organization; 1986.
6. Phadke, MS. Quality engineering using robust design. Englewood Cliffs, NJ: Prentice Hall; 1989.
7. Itasca Consulting Group. Flac3d—fast lagrangian analysis of continua in 3 dimensions: User's guide, version 5.01. Minneapolis: Itasca Consulting Group, Inc; 2013.
8. Devore, JL. Probability and statistics for engineering and the sciences. 5. Pacific Grove, CA: Duxbury Thomson Learning; 2000.
9. Mendenhall, W., Sincich, T. Statistics for engineering and the sciences. 4. Englewood Cliffs, NJ: Prentice-Hall; 1995.
10. Marinos P, Hoek E. Estimating the geotechnical properties of heterogeneous rock masses such as flysch. Bull Eng Geol Environ. 2001; 60:85–92.
11. Harr, ME. Reliability-based design in civil engineering. McGraw-Hill; 1987.
12. Farmer, IW. Engineering properties of rocks. London: E.&F. N. Spon; 1968.
13. Palisade Corporation. @risk®, risk analysis using monte carlo simulation. ver. 7.5.1. Ithaca, NY: Palisade Corporation; 2016.
14. Hoek, E., Carranza-Torres, C., Corkum, B. Hoek-brown failure criterion-2002 edition. Proceedings of the 5th North American rock mechanics symposium and the 17th tunnelling association of Canada conference: NARMS-TAC 2002-mining and tunnelling innovation and opportunity; Toronto, Ontario, Canada. July 7–10; p. 267-73.
15. Kim B-H, Larson MK. Assessment of bump-prone potential and numerical investigation on brittle failure mechanisms associated with floor heave in a coal mine. J Southern Afr Inst Min Metall. 2017 submitted for publication.
16. Agapito, JFT., Gilbride, L., Koontz, W. Implication of highly anisotropic horizontal stresses on entry stability at the west elk mine, somerset, colorado. Proceedings: 24th international conference on ground control in mining; Morgantown, WV. August 2–4; p. 196-202.

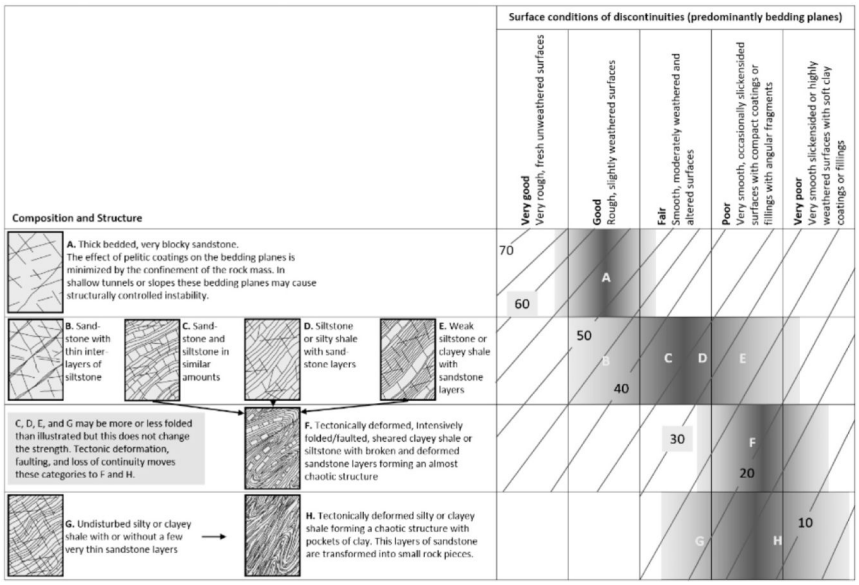

Fig. 1.
Geological strength index (GSI) chart for heterogeneous rock masses [after 10].

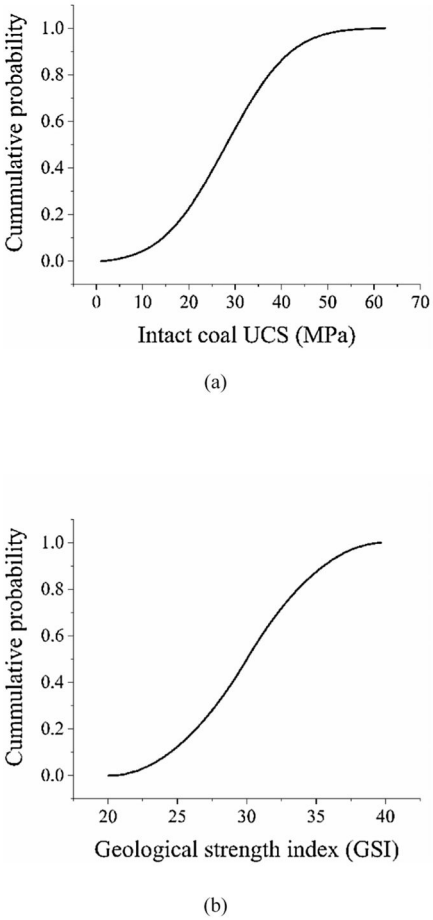

Fig. 2.
Cumulative probability distributions for intact coal UCS (a) and GSI (b).

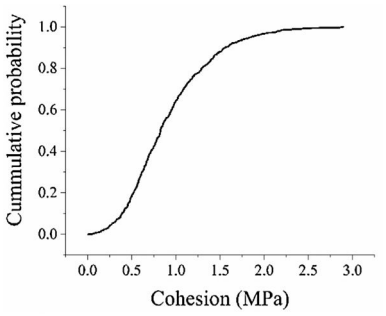

(a)

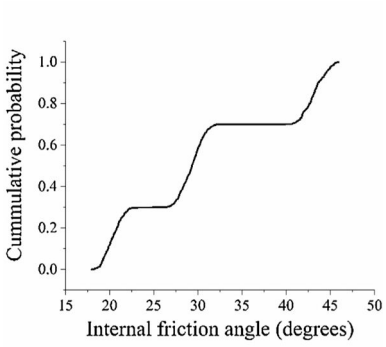

(b)

Fig. 3.

Cumulative probability distributions for cohesion (a) and internal friction angle (b) for the rock mass of coal estimated by Monte Carlo simulation.

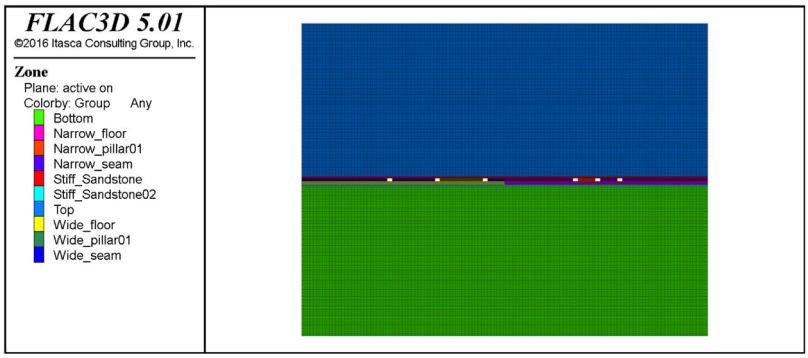

(a) Case 1

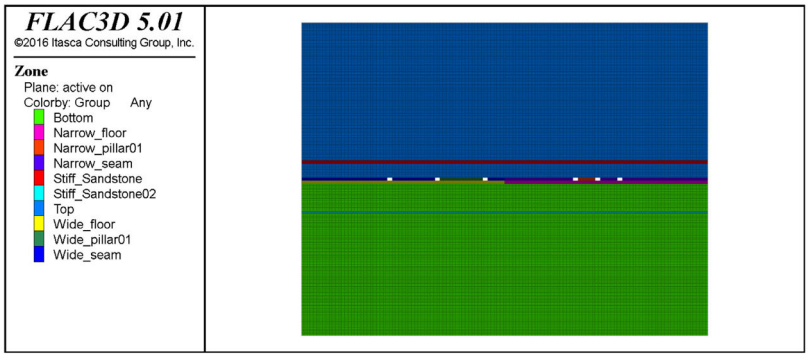

(b) Case 16

Fig. 4.
Examples of FLAC3D model as per experimental number generated by orthogonal array.

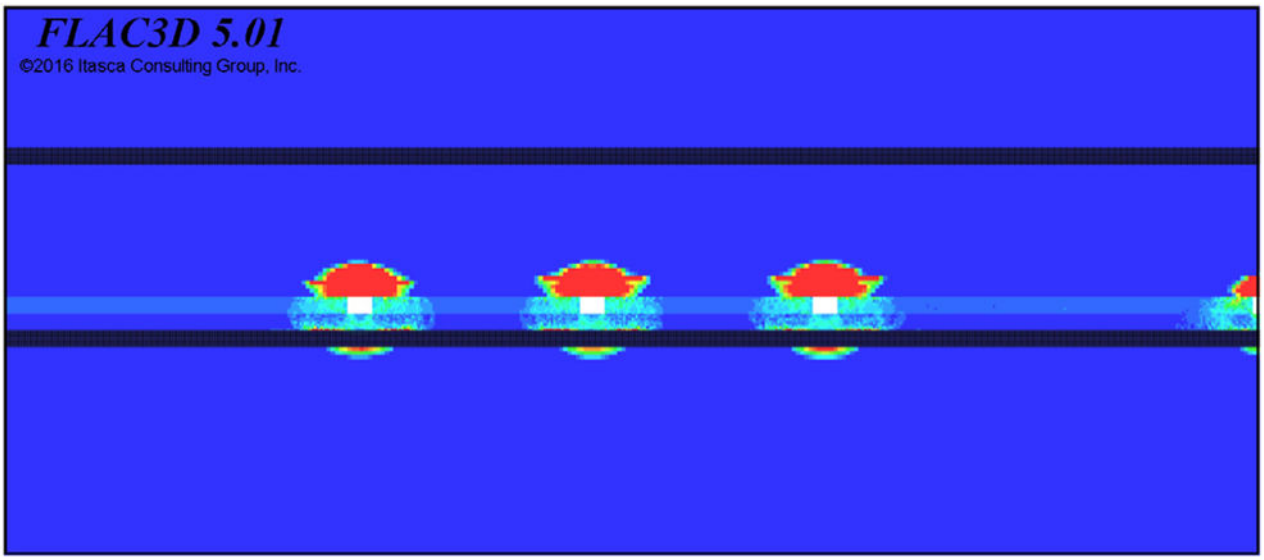

Fig. 5.
Maximum plastic energy dissipated in wide roof (Case 7, 28% increased).

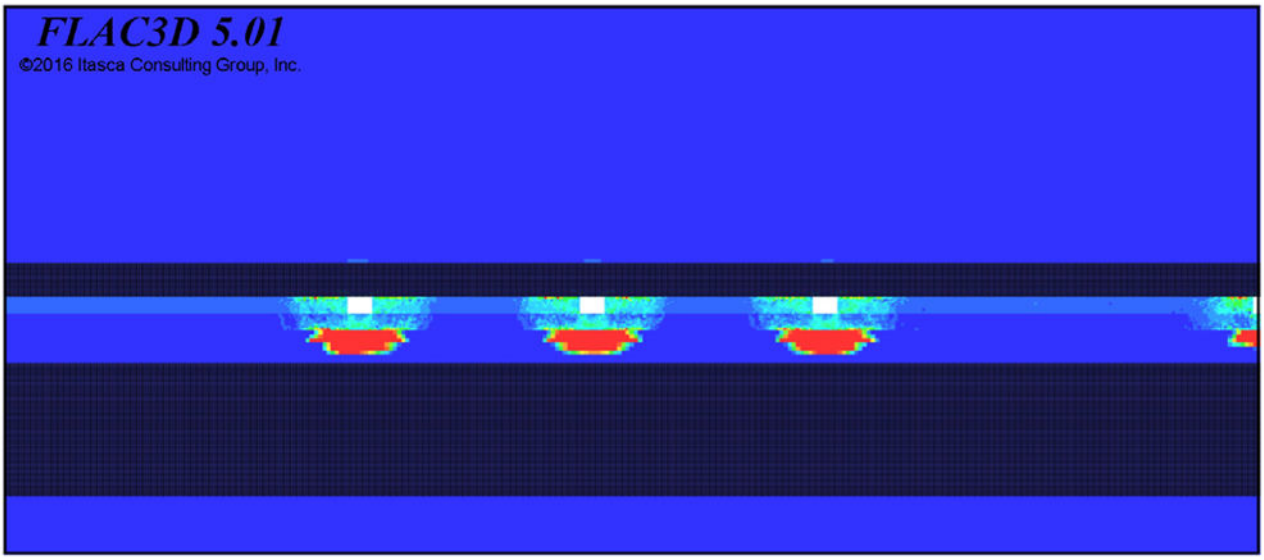

Fig. 6.
Maximum plastic energy dissipated in wide pillar (Case 15, 18% increased).

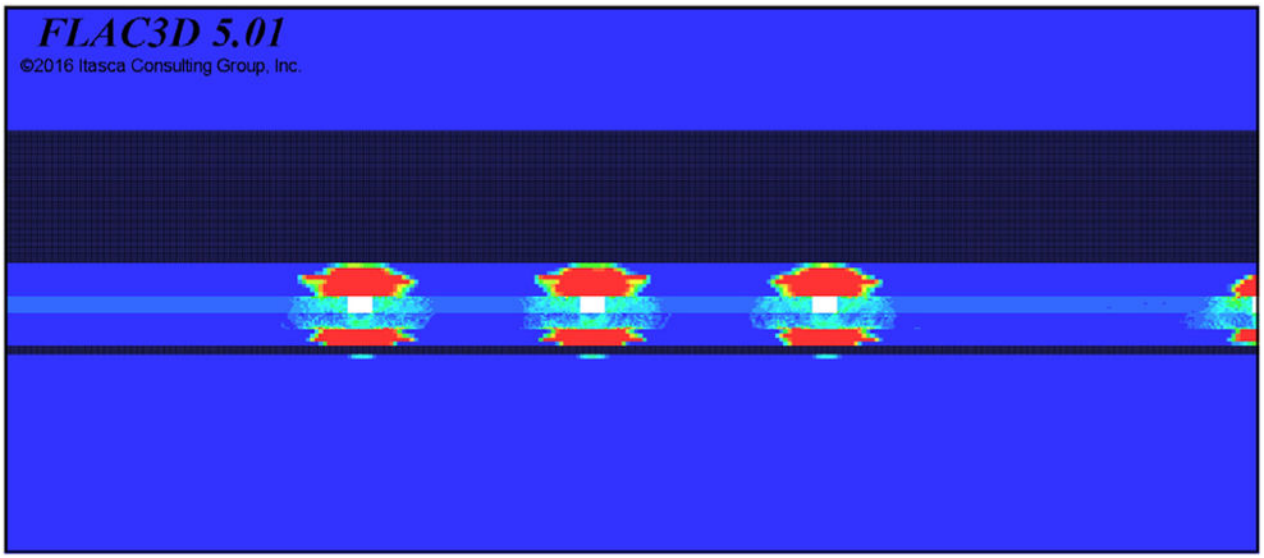

Fig. 7.
Maximum plastic energy dissipated in wide floor (Case 21, 12% increased).

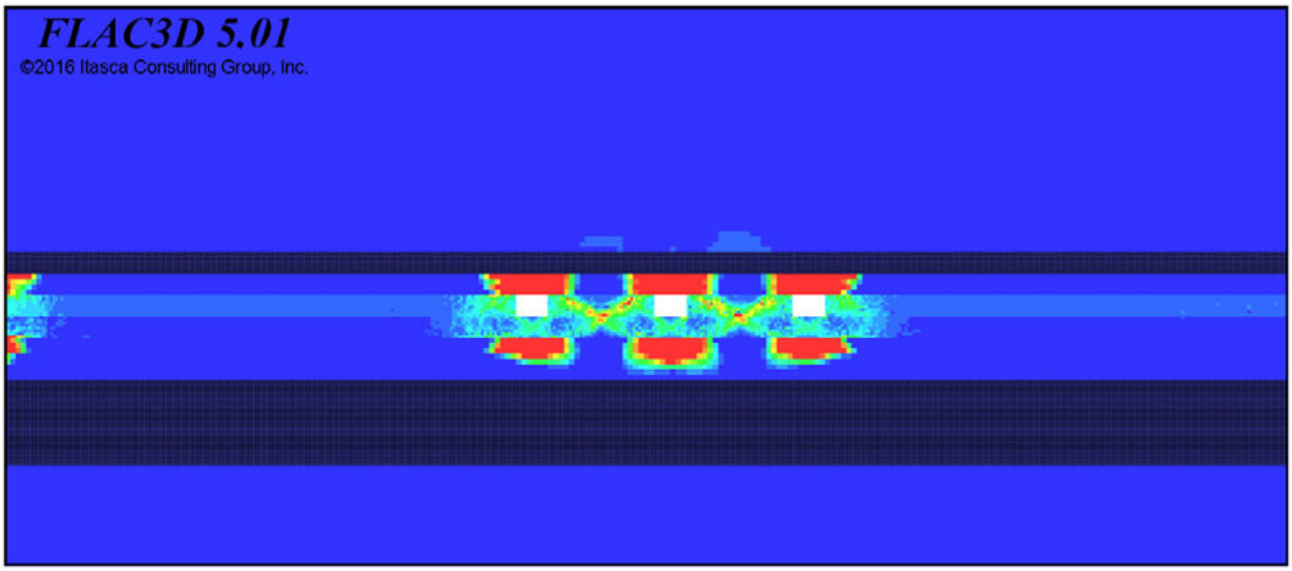

Fig. 8.
Maximum plastic energy dissipated in narrow roof (Case 9, 7% increased).

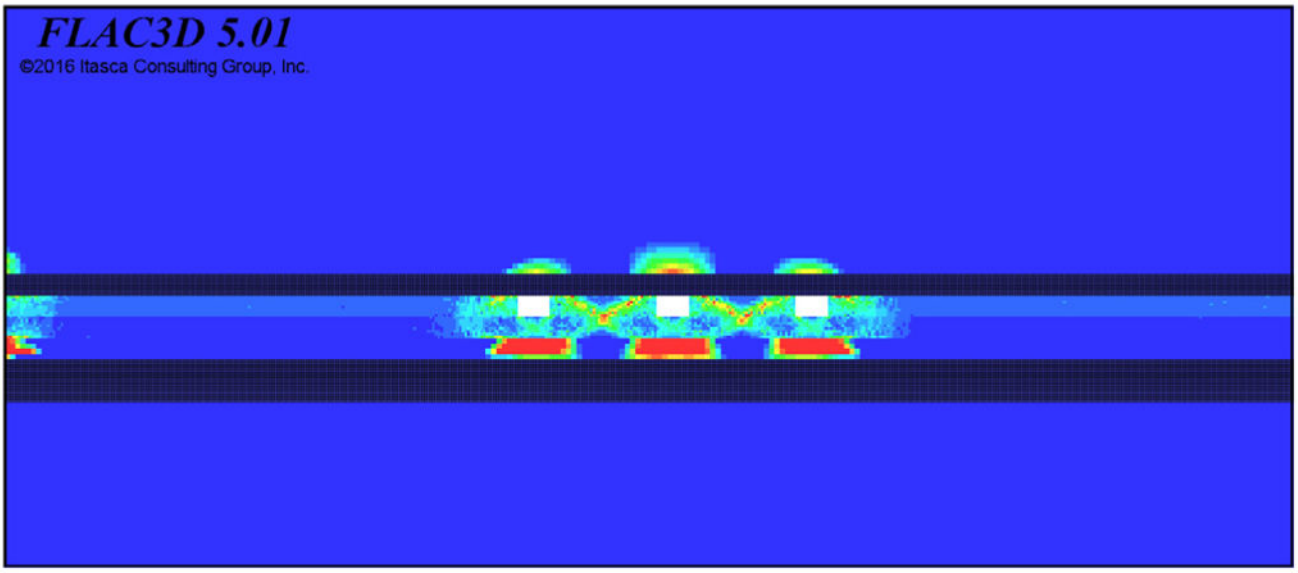

Fig. 9.
Maximum plastic energy dissipated in narrow pillar (Case 8, 8% increased).

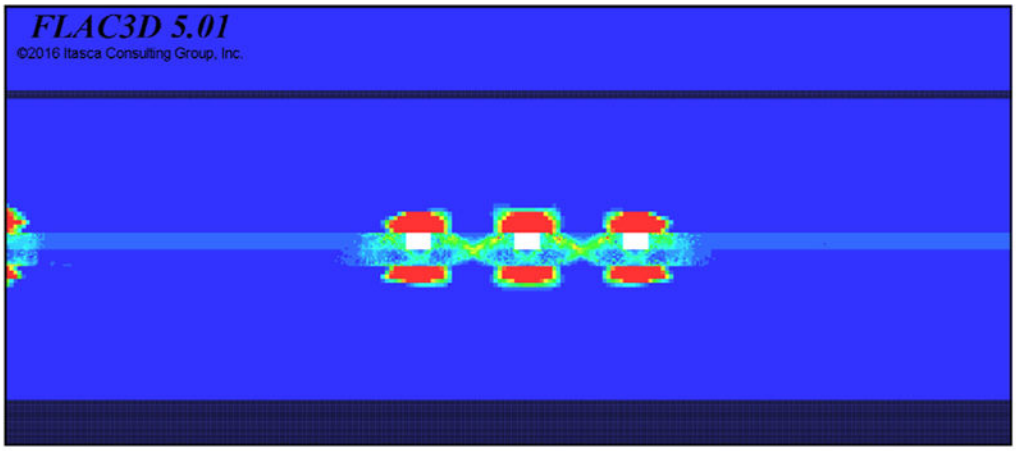

Fig. 10.
Maximum plastic energy dissipated in narrow floor (Case 5, 21% increased).

Table 1

Estimated material properties for the rock masses.

Input parameter	Rock mass type	Value
Unit weight	Stiff sandstone	0.027 MN/m^3
	Coal seam	0.022 MN/m^3
	Rock masses in top and bottom	0.027 MN/m^3
Young's modulus	Stiff sandstone	13.5 GPa
	Coal seam	0.8 GPa
	Rock masses in top and bottom	11.7 GPa
Poisson's ratio	Stiff sandstone	0.25
	Coal seam	0.30
	Rock masses in top and bottom	0.25
Cohesion	Stiff sandstone	2.4 MPa
	Coal seam	1.0 MPa
	Rock masses in top and bottom	1.1–1.5 MPa
Internal friction angle	Stiff sandstone	54°
	Coal seam	26°
	Rock masses in top and bottom	41°
Tensile strength	Stiff sandstone	0.20 MPa
	Coal seam	0.01 MPa
	Rock masses in top and bottom	0.10 MPa

Table 2

Orthogonal array, $L_{25}(5^6)$ for FLAC3D modeling.

Experimental case No.	Thickness of stiff sandstone in top (m)	Thickness of stiff sandstone in bottom (m)	Friction angle of interfaces (°)	Modulus of stiff sandstone (GPa)	Distance of stiff sandstone from the roof of seam (m)	Distance of stiff sandstone from the floor of seam (m)
1	2	2	40	13.5	0	0
2	2	4	45	21.9	4	4
3	2	8	50	24.9	8	8
4	2	16	55	33.5	16	16
5	2	32	60	41.9	32	32
6	4	2	45	24.9	16	32
7	4	4	50	33.5	32	0
8	4	8	55	41.9	0	4
9	4	16	60	13.5	4	8
10	4	32	40	21.9	8	16
11	8	2	50	41.9	4	16
12	8	4	55	13.5	8	32
13	8	8	60	21.9	16	0
14	8	16	40	24.9	32	4
15	8	32	45	33.5	0	8
16	16	2	55	21.9	32	8
17	16	4	60	24.9	0	16
18	16	8	40	33.5	4	32
19	16	16	45	41.9	8	0
20	16	32	50	13.5	16	4
21	32	2	60	33.5	8	4
22	32	4	40	41.9	16	8
23	32	8	45	13.5	32	16
24	32	16	50	21.9	0	32
25	32	32	55	21.9	4	0

Table 3

Normalized floor displacement and plastic dissipated energy measured in different locations.

Case No.	Dissipated energy (wide pillar)	Dissipated energy (narrow pillar)	Dissipated energy (wide roof)	Dissipated energy (narrow roof)	Dissipated energy (wide floor)	Dissipated energy (narrow floor)
1	1.000	1.000	1.000	1.000	1.000	1.000
2	0.866	1.020	1.218	1.290	1.108	1.105
3	0.789	1.057	1.246	1.032	1.007	1.170
4	0.821	0.874	1.122	1.038	1.035	1.192
5	0.696	1.031	1.150	1.043	1.051	1.208
6	0.858	1.009	1.113	1.081	1.042	1.169
7	0.792	0.935	1.275	1.037	0.650	0.439
8	1.129	1.084	0.962	0.334	1.117	1.122
9	0.894	1.066	1.219	1.354	1.040	1.162
10	0.777	0.827	1.126	1.033	1.026	1.177
11	0.777	0.956	1.138	1.107	1.036	1.202
12	1.081	0.612	0.445	0.109	0.361	0.296
13	0.797	0.927	1.146	1.023	0.579	0.427
14	0.842	0.806	1.110	1.043	1.053	1.168
15	1.184	0.922	0.034	0.054	0.991	1.174
16	0.793	0.909	1.155	1.045	1.026	1.159
17	0.958	0.938	0.038	0.038	1.014	1.201
18	0.769	0.814	1.111	1.083	1.040	1.176
19	0.696	0.729	1.228	1.018	0.474	0.279
20	1.096	0.952	1.096	1.059	1.045	1.197
21	0.995	0.785	1.208	1.015	1.122	1.116
22	0.878	0.769	1.132	1.027	1.009	1.152
23	1.000	0.988	1.109	1.046	1.059	1.206
24	1.051	0.822	0.045	0.042	1.011	1.190
25	0.677	0.618	1.119	0.971	0.459	0.324

Table 4

Calculated coefficient of variation.

	Dissipated energy (wide pillar)	Dissipated energy (narrow pillar)	Dissipated energy (wide roof)	Dissipated energy (narrow roof)	Dissipated energy (wide floor)	Dissipated energy (narrow floor)
Coefficient of variation	0.162	0.145	0.395	0.457	0.242	0.334

Table 5

Correlation matrix by principal component analysis.

	Dissipated energy (wide pillar)	Dissipated energy (narrow pillar)	Dissipated energy (wide roof)	Dissipated energy (narrow roof)	Dissipated energy (wide floor)	Dissipated energy (narrow floor)
Dissipated energy (wide pillar)	1.000					
Dissipated energy (narrow pillar)	0.143	1.000				
Dissipated energy (wide roof)	−0.607	0.159	1.000			
Dissipated energy (narrow roof)	−0.630	0.207	0.928	1.000		
Dissipated energy (wide floor)	0.243	0.616	0.035	0.151	1.000	
Dissipated energy (narrow floor)	0.252	0.547	−0.086	0.058	0.970	1